Superlattices and Microstructures 85 (2015) 237–247

Contents lists available at ScienceDirect

Superlattices and Microstructures

journal homepage: www.elsevier.com/locate/superlattices

Structural, morphological characteristics and optical properties of Y doped ZnO thin films by sol–gel spin coating method

M. Thirumoorthi [a], J. Thomas Joseph Prakash [b,*]

[a] PG and Research Department of Physics, H.H. The Rajah's College (Affiliated to Bharathidasan University), Pudukkottai 622 001, India
[b] Department of Physics, Government Arts College (Affiliated to Bharathidasan University), Trichy 620 022, India

ARTICLE INFO

Article history:
Received 24 April 2015
Accepted 5 May 2015
Available online 21 May 2015

Keywords:
Thin film
Sol–gel method
X-ray diffraction
Surface morphology
Optical properties

ABSTRACT

Un-doped and Y doped ZnO thin films were deposited successfully by sol–gel spin coating method with different Y concentrations. The X-ray diffraction spectra revealed that all the films have poly-crystalline of hexagonal wurtzite structure. SEM images of the films show different micro structure with nano clusters and show a reduction in surface roughness. The EDX spectrum confirms the presence of Zn, O and Y elements in the prepared films. The optical transmittance spectrum indicates the average transmittance of the films is increased from 78% to 83%. The optical band gaps of the ZnO films were changed from 3.33 eV to 3.43 eV with increasing Y doping. PL spectra show the blue shift in near band edge (NBE) UV emission. The presence of functional groups and the chemical bonding is confirmed by FTIR spectra. The Hall measurements show that the films have *n*-type conductivity.

© 2015 Elsevier Ltd. All rights reserved.

1. Introduction

Zinc oxide (ZnO) is one of the transparent conducting oxide (TCO) materials whose thin films attract much interest because of typical properties such as high optical transparency in the visible and near-infrared region and electrical properties. Due to these properties ZnO is a promising material

* Corresponding author.
E-mail address: armyjpr1@yahoo.co.in (J. Thomas Joseph Prakash).

http://dx.doi.org/10.1016/j.spmi.2015.05.005
0749-6036/© 2015 Elsevier Ltd. All rights reserved.

Nomenclature

β	full width at half maximum (rad)
D	crystallite size (nm)
λ	wavelength of X-ray (Å)
θ	Bragg's angle (deg)
d	lattice spacing (Å)
ε	micro-strain
h, k, l	miller indices
L	bond length (Å)
V	volume of unit cell (Å)
α	absorption coefficient
T	transmittance (%)
hv	photon energy (eV)
Eg	optical band gap (eV)
ρ	resistivity (Ω cm)
n	carrier concentrations (cm^{-3})
μ	mobility (cm/Vs)

for optoelectronic applications such as solar cells, gas sensors, liquid crystal displays and thin film transistors [1–3]. ZnO is an II–VI wide band gap semiconductor which has a band gap ~ 3.37 eV at room temperature and large excitonic binding energy ~60 meV. As required by its applications, its electrical conductivity and optical transmittance can be tuned by doping with various dopants such as gallium, aluminum, fluorine, indium and tin [4–8]. In recent years, rare earth elements have been of great interest as dopant sources for ZnO because they can reduce the native point defect densities in ZnO [9,10]. The Y-doped ZnO (YZO) has been of ample interest because Y improves the optical and the electrical properties. For example, Kaur et al. [11] demonstrated the use of Y-doped ZnO as a transparent window layer for thin film solar cells. In their study, the sheet resistance and average transmittance was decreases as function of thickness. Yang et al. [12] demonstrated the Tunable deep-level emission of ZnO nanoparticles using yttrium doping. Heo et al. [13] reported that the densities of oxygen-related native point defects are minimized, and the crystallite sizes of YZO grains are maximized. Mariappan et al. [14] observed a reduction of band gap when Y is doped with ZnO. The Y doped ZnO thin films have been prepared using different techniques such as nebulizer spray pyrolysis method [14], DC magnetron sputtering [15], pulsed laser deposition [16] and sol–gel process [11,13]. The sol–gel method has some merits, such as the easy control of chemical components, and fabrication of thin film at a low cost. In this study, we successfully prepared the Y-doped ZnO thin films by the sol–gel spin coating method and investigated in detail the effects of Y doping on the structural, morphological, optical, photoluminescence (PL), FTIR and electrical properties of ZnO thin films.

2. Experimental

Un-doped and Y doped ZnO thin films were deposited by sol–gel spin coating method onto glass substrates. Zinc acetate di-hydrate, 2-methoxyethanol and mono-ethanolamine (MEA) were used as a starting material, solvent and stabilizer, respectively. The molar ratio of MEA to zinc acetate dehydrate was maintained at 1.0 and the concentration of zinc acetate was 0.3 M. For yttrium doping, the yttrium tri-chloride was added to the solution at the concentrations of 0, 5, and 10 wt.%. The resultant solution was stirred at 60 °C for 1 h to yield a clear and homogeneous solution. The films were prepared on ultrasonically cleaned glass substrates using spin-coating (HOLMARC) unit which was rotated at 3000 rpm for 30 s. After spin coating, the film was dried at 120 °C for 10 min to evaporate the solvent and remove organic residuals. The procedures from coating to drying were repeated 5 times to obtain optimum thickness. The film was then inserted into a furnace and annealed in air at 500 °C for 1 h.

The structure and lattice parameters of prepared films were analyzed by X-ray diffractometer (XRD) using the PANalytical system with Cu $K\acute{\alpha}_1$ radiation (λ = 1.54056 Å). Surface morphology was examined by the Scanning Electron Microscope (ESEMQUANTA200, FEI-Netherland). Elemental analysis was made by energy dispersive X-ray spectroscopy (attached to SEM). The variations of surface roughness were analyzed by microphotographs (FUJIFILM FinPix S3300) and the contact angle measured using protractor. The optical properties of ZnO films were carried out with a double beam spectrophotometer (Oceans optics HR2000-USA) in the UV–Visible regions. The photoluminescence (PL) measurements were performed using a spectrofluorometer (Cary Eclipse EL08083851) with xenon arc lamp. The IR spectrum was recorded using FTIR spectrophotometer (Perkin Elmer – RX I) in the range of 400–4000 cm^{-1}. The electrical parameters of prepared samples were collected from room temperature Hall Effect measurements using the RH2035 PhysTech GmbH system.

3. Result and discussions

3.1. Structural properties

Fig. 1 shows the X-ray diffraction pattern of Y-doped ZnO thin films with different Y concentrations deposited at 500 °C. The XRD patterns of the films revealed almost all the characteristic peaks that correspond to bulk ZnO, namely the (100), (002), (101) and (110) reflections. It can be observed that these prepared films are polycrystalline of hexagonal wurtzite structure according to standard X-ray diffraction data (JCPDS file No. 89-1397). All the films show a preferential orientation along the (101) plane. These observations are in agreement with previous reported results [12,17,18]. The increasing of the intensity of (101) diffraction peak is related to the improvement in the crystalline quality of the films with the increasing Y concentrations. There are no extra peaks corresponding to Y related secondary and impurity phases, which may be attributed to the Y are incorporated into Zn sites or interstitial sites.

The average crystallite sizes (D) of the prepared films have been calculated using Scherrer's equation as given below [18]

$$D = \frac{0.9\lambda}{\beta \cos \theta} \tag{1}$$

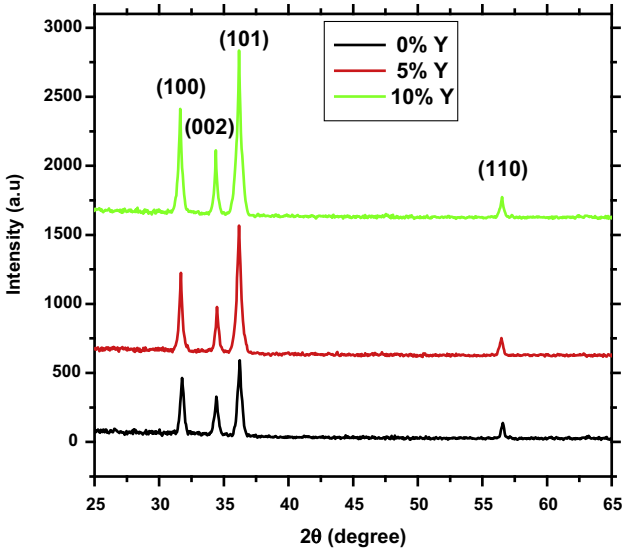

Fig. 1. X-ray diffraction patterns of ZnO:Y thin films for different concentrations.

where λ, β and θ are the X-ray wavelength (1.54060 Å), full width at half maximum (FWHM) and Bragg's diffraction angle of (1 0 1) plane in degrees respectively.

The micro-strain (ε) can be calculated using the formula [18],

$$\varepsilon = \frac{\beta \cos \theta}{4} \tag{2}$$

The dislocation density (δ) of prepared films are calculated using the relation [14],

$$\delta = \frac{1}{D^2} \tag{3}$$

The lattice constants '*a*' and '*c*' for ZnO films are estimated using the following relation [14]

$$1/d^2 = \frac{4}{3}\left[\frac{[h^2 + hk + k^2]}{a^2}\right] + \frac{l^2}{c^2} \tag{4}$$

The Zn–O bond length (L) has been calculated using the following relationship [6],

$$L = \sqrt{(a^2/3) + ((1/2) - u)^2 c^2} \tag{5}$$

where $u = (a^2/3c^2) + 0.25$ is the potential parameter of the hexagonal structure. The volume (V) of unit cell of hexagonal system has been calculated from the equation [19].

$$V = 0.866 \times a^2 \times c \tag{6}$$

Table 1 shows obtained values of *d*-space, grain size, dislocation density, strain, lattice constants, and bond length. The crystallite sizes were changed from 26.21 nm to 37.94 nm as varying Y concentrations confirming improvement in the crystalline quality. The dislocation density (δ) is measures the defects in the crystal structure. The obtained value for ZnO films is decreased with Y doping, which means Y doping reduce the lattice defects in the ZnO films. The observed shrinkage in strain is related to the change in shape of the particles and indicates reduction of point defects. The obtained values of *d*-space and lattice constants are agreed with the standard values [JCPDS card No: 89-1397]. The observed reduction in '*c*' value for Y-doped ZnO films may due to decreased residual stress. The change in peak intensity, d-value, lattice constants, bond length and volume confirms the substitution of Y into Zn–O lattice.

3.2. Surface morphology

Fig. 2 shows the scanning electron microphotographs and microphotographs of water droplet on surface of prepared ZnO thin films with different Y concentrations. Surface of all the films shows different micro structure with nano clusters. The un-doped ZnO film has hierarchical rough surface with randomly distributed particles. The surface of the Y-doped ZnO films show rough surface with uniform distribution of particles.

Table 1
Structural parameters of ZnO thin films with different Y concentrations.

Sample	2θ value (deg)	*d*-space (Å)	Average crystallite size (nm)	Dislocation density (δ) (10^{14}) (lines/m)	Strain (ε) (10^{-4})	Bond length (L) (Å)	Volume (V) (Å^3)	Lattice constants	
								a	*c*
Zn:Y (0%)	36.22	2.4781	26.21	14.51	13.22	1.9805	47.82	3.2490	5.2318
Zn:Y (5%)	36.17	2.4814	31.43	10.12	11.02	1.9822	47.93	3.2590	5.1913
Zn:Y (15%)	36.17	2.4814	37.94	06.94	09.13	1.9805	47.78	3.2646	5.1774
JCPDS file No: 89-1397	36.21	2.4784	–	–	–	–	–	3.2530	5.2130

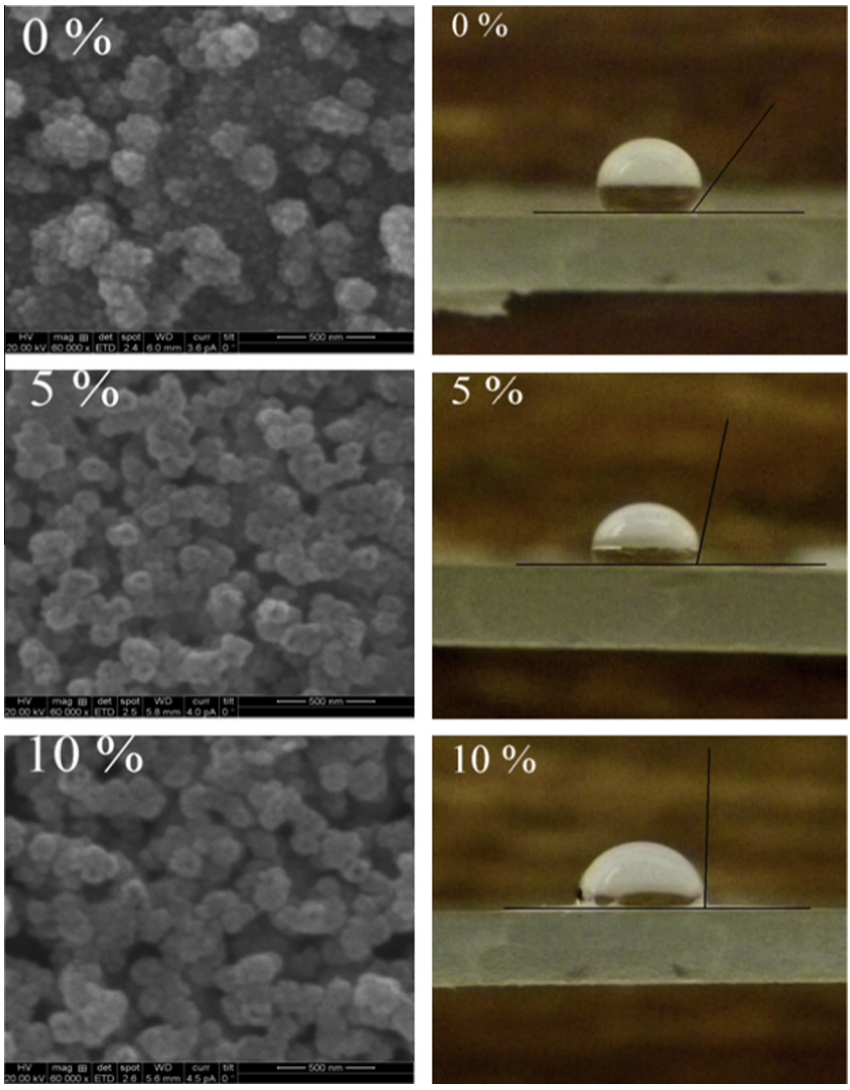

Fig. 2. Surface morphologies of ZnO:Y thin films with different concentrations and microphotograph of water droplet on surface of respective films.

From the microphotographs of water droplet on the surface, it can be seen that the contact angles (∼141°, 108°, 92° for 0%, 5%, and 10% respectively) for water droplet changed with Y doping. The change in water contact angle indicating the increase of hydrophilicities and reduction of surface roughness. Fig. 3 shows the schematic diagram of variations of water contact angle for different surface structure. It suggests that the water contact angle is improved as increasing roughness of the surface due to low surface energy. The smooth surface may help to improve the optical transmittance.

The energy dispersive X-ray spectroscopy (EDX) of un-doped and Y-doped ZnO films is shown in Fig. 4. The spectrum confirms presence of Zn, O and Y elements in the prepared films with their nominal percentage.

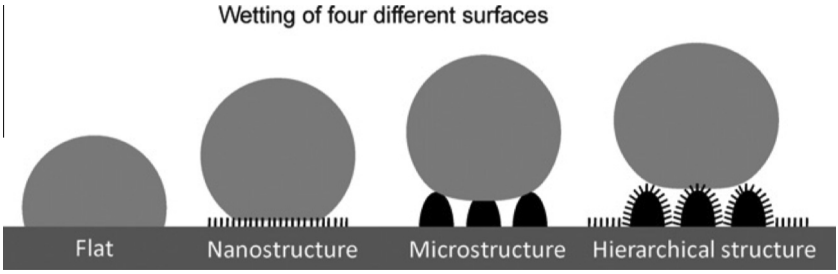

Fig. 3. Schematic diagram of different surface structure.

3.3. Optical properties

The optical transmittance spectra of the Y-doped ZnO thin films are presented in Fig. 5 for the wavelength range of 300–1000 nm. It can be seen that the optical transmittance in the visible range is 78%, 83% and 82% for 0%, 5%, and 10 wt.% of Y doped ZnO films, which is comparatively higher then reported results [11,14,20]. This result suggests that the optical quality of Y doped ZnO films are improved, which may due to low scattering or low absorption. The absorption edge of the ZnO film shifts to smaller wavelengths. From these results, it is evident that doping of Y with ZnO helps to develop the transmittance in the visible region.

The optical band gaps of the films are calculated from the transmittance spectra employing Tauc's plot as shown in Fig. 6((a)–(c)). The absorption coefficient (α) is calculated using the equation [21],

$$\alpha = \frac{1}{d}\ln(1/T) \tag{7}$$

where T is transmittance and d is film thickness. The absorption coefficient (α) and the incident photon energy ($h\nu$) is related by the following equation [21],

$$(\alpha h\nu)^2 = A(h\nu - \mathrm{Eg}) \tag{8}$$

where A and Eg are constant and optical band gap respectively. The obtained band gap values were plotted as function of Y concentrations is shown in Fig. 6(d). It can be seen that the band gap of ZnO thin films is increased from 3.33 to 3.44 eV. The blue shift in band gap is arises because the Fermi level lies inside the conduction band for n-type doping, which related to Mass–Burstein effect [22]. A similar result was reported in the previous literature for Y-doped ZnO nano particles [18].

3.4. Photoluminescence

Room temperature photoluminescence spectrum of un-doped and Y-doped ZnO thin films were recorded under the excitation wavelength λ = 371 nm is shown in Fig. 7. Mainly four emission peaks is observed in photoluminescence spectrum. A strong UV emissions peak centered at ~414 nm, a weak blue band at ~456 nm, a strong blue-green band at ~491 nm and a weak green band at ~507 nm. The strong UV emission peak originates from the recombination of free excitons related to the near-band edge emission of ZnO. The observed blue shift (Fig. 7 insert) in the UV emission peak is due to the Burstein–Moss effect [22]. The blue emission peak at 456 nm correspond to the emission due to neutral and ionized zinc vacancy related defects [23]. The blue-green emissions are possibly due to surface defects of the prepared film. The green emission peak at 507 nm is due to radial recombination of the photo-generated hole with the electrons that belongs to the singly ionized oxygen vacancies [24]. A rapid decrease in the intensity of all peaks after Y incorporation and observed blue shift in UV emission peak confirms the substitution of Y ion in the ZnO lattice.

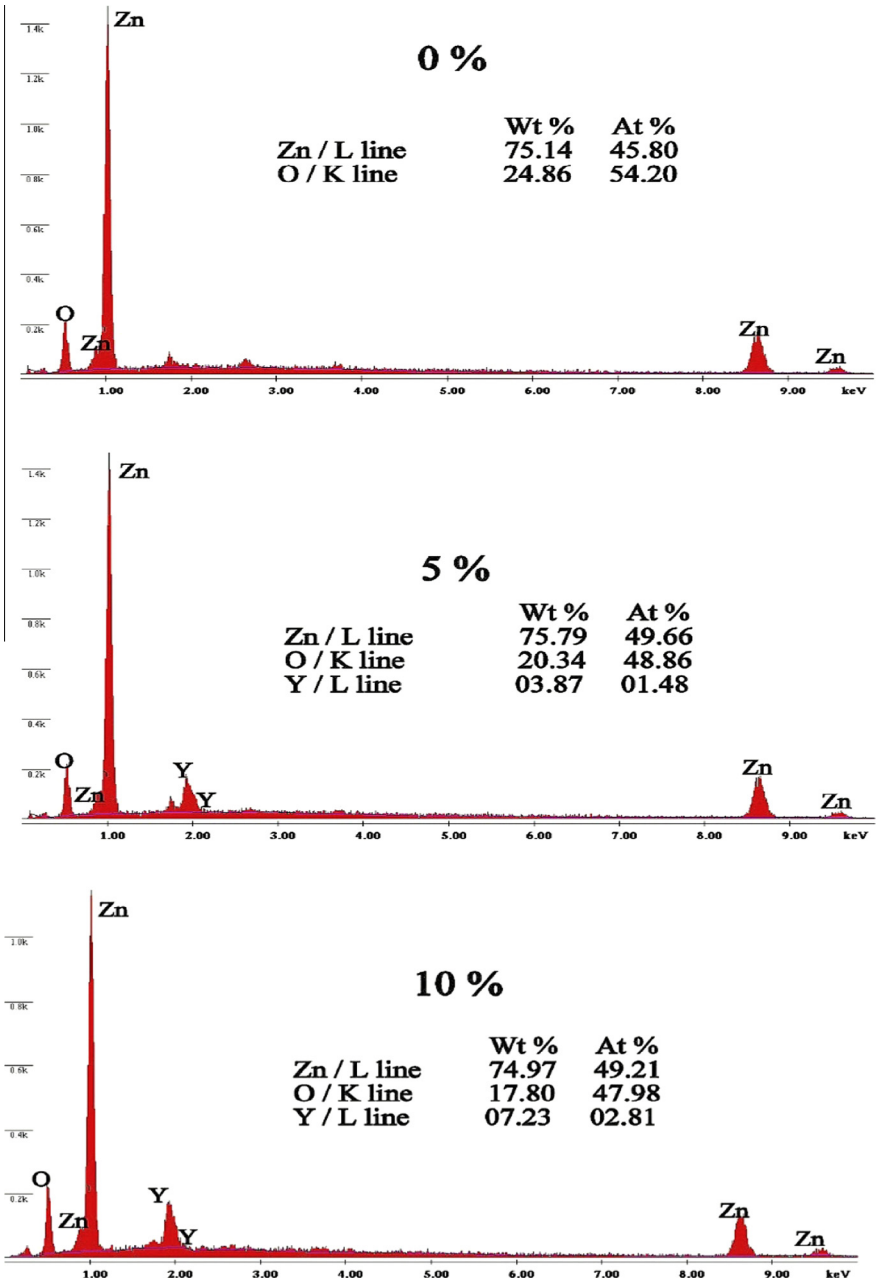

Fig. 4. EDX spectrum of ZnO:Y thin films.

3.5. FTIR analysis

FTIR is a technique used to obtain the information regarding chemical bonding in a material. The band positions and numbers of absorption peaks are dependent on crystalline structure, chemical composition and morphology of the films also [25]. The FTIR spectrum of un-doped and Y-doped

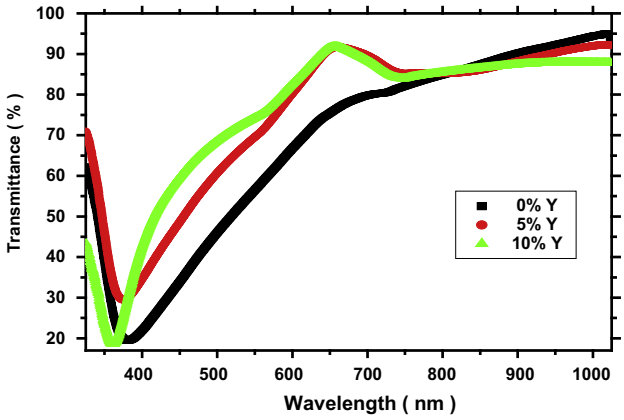

Fig. 5. UV–Visible transmittance spectrum of ZnO:Y thin films.

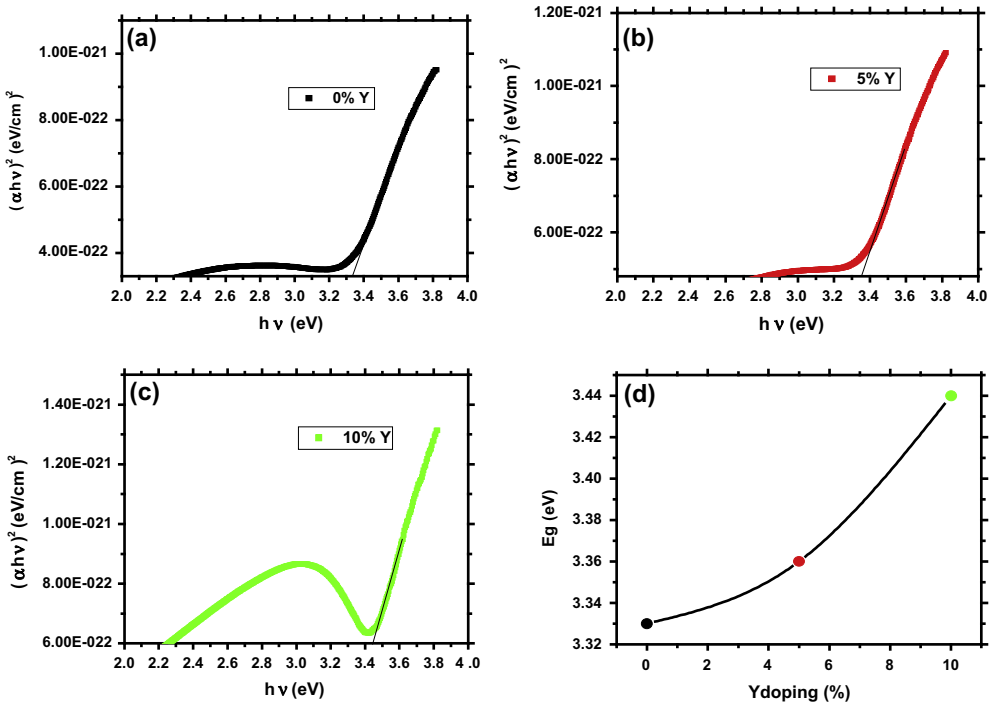

Fig. 6. The plots of $(\alpha h\nu)^2$ vs. incident photon energy ($h\nu$); (a) 0%, (b) 5%, (c) 10% and (d) obtained band gap (Eg) of the ZnO thin films as function of Y concentrations.

ZnO thin films is shown in Fig. 8. The broad absorption bands around 3488 cm^{-1} were attributed to the normal polymeric O–H stretching vibration of water molecule in Zn–O lattice. A small band around 1604 cm^{-1} is assigned to bending H–O–H vibration of the water molecules absorbed on the surface of ZnO [26]. The characteristic IR peaks below 633 cm^{-1} is ascribed to presence of ZnO–Y bond. The band occurring near 727 cm^{-1} is attributed to the vibrations of Y–ZnO local bond [18].

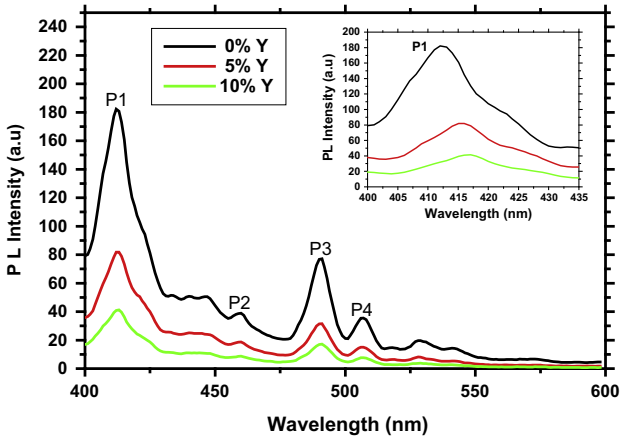

Fig. 7. Room temperature photoluminescence of ZnO:Y thin films. The insert shows the blue shift of UV emissions peak.

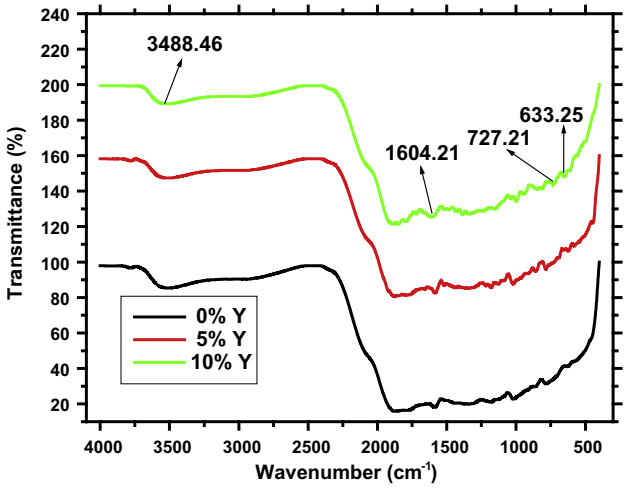

Fig. 8. FTIR spectrum of un-doped and Y doped ZnO thin films.

3.6. Electrical properties

Fig. 9 shows the influence of Y-doping on electrical resistivity (ρ), carrier concentration (n) and mobility (μ) of ZnO thin films. The Hall measurements show that the films have n-type conductivity. The electrical resistivity is found to decrease from 3.2×10^{-2} Ω cm to 4.3×10^{-3} Ω cm and the carrier concentration increased gradually from 6.3×10^{19} cm^{-3} to 2.4×10^{20} cm^{-3} for 0–10% of Y doping. The obtained resistivity is lower than the reported values [13,27]. The mobility was increased from 1.6 to 3.9 cm/Vs for 0–5% doping and then decreased to 3.6 cm/Vs for 10% of Y doping. A minimum resistivity and maximum carrier concentration is obtained for 10% of Y-doped ZnO film. The decrease in resistivity with the increasing Y concentration can be attributed to the increase in the carrier concentration, mobility of the charge carriers and grain boundary scattering. The increase of carrier concentration of Y doped ZnO thin films may due to the contribution of extra free carriers of Y^{3+} ions substituting Zn^{2+} ions.

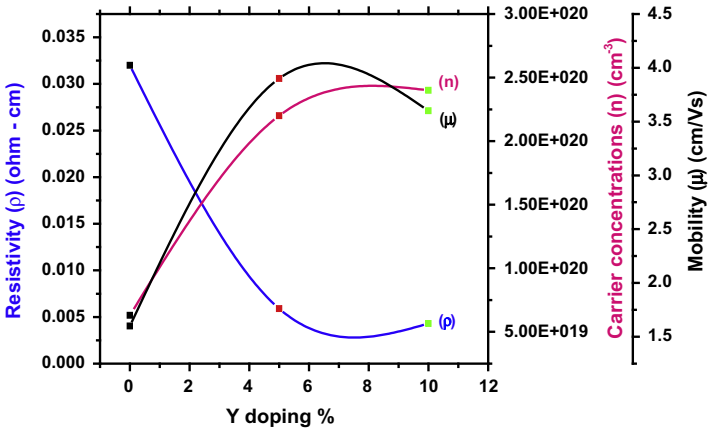

Fig. 9. Electrical resistivity (ρ), carrier concentration (n), and mobility (μ) of ZnO thin films as function of Y concentrations.

4. Conclusion

The following are the conclusions drawn from the present investigation:

- Transparent conducting Y-doped ZnO thin films were fabricated by sol–gel spin coating method. XRD results show that all the films are polycrystalline in nature with hexagonal wurtzite structure.
- SEM images of the films show different micro structure with nano clusters. The surface was strongly influenced by Y doping with ZnO films and observed a reduction in surface roughness. The EDX spectrums confirm the presence of Zn, O and Y elements in the prepared films.
- We observed an improvement in optical transmittance for Y-doped ZnO thin films in visible region (78–83%). The optical band gap of films shows a blue shift with Y doping.
- The diminishing photoluminescence peak intensity and observed blue shift of UV emissions peak is revealed that substitutions Y into ZnO systems.
- The presence of functional groups and chemical bonding were confirmed by FTIR.
- The Hall measurements show that improvements in electrical properties and films have *n*-type conductivity.

From these results, the Y doped-ZnO thin films may be a potential candidate for optoelectronic applications.

References

[1] M. Girtan, A. Vlad, R. Mallet, M.A. Bodea, J.D. Pedarnig, A. Stanculescu, D. Mardare, L. Leontie, S. Antohe, On the properties of aluminium doped zinc oxide thin films deposited on plastic substrates from ceramic targets, Appl. Surf. Sci. 274 (2013) 306–313.
[2] J.Q. Xu, Q.Y. Pan, Y.A. Shun, Z.Z. Tian, Grain size control and gas sensing properties of ZnO gas sensor, Sens. Actuators, B 66 (2007) 277–279.
[3] Sayantan Das, Rajitha N.P. Vemuri, T.L. Alford, Enhanced conductivity of Y-doped ZnO thin films by incorporation of multiple walled carbon nanotubes, Thin Solid Films 527 (2013) 92–95.
[4] Chang-Feng Yua, Sy-Hann Chena, Shih-Jye Sunb, Hsiung Chou, Influence of the grain boundary barrier height on the electrical properties of Gallium doped ZnO thin films, Appl. Surf. Sci. 257 (2011) 6498–6502.
[5] Amita Verma, F. Khan, D. Kumar, M. Kar, B.C. Chakravarty, S.N. Singh, M. Husain, Sol–gel derived aluminum doped zinc oxide for application as anti-reflection coating in terrestrial silicon solar cells, Thin Solid Films 518 (2010) 2649–2653.
[6] Saliha Ilican, Yasemin Caglar, Mujdat Caglar, Fahrettin Yakuphanoglu, Structural, optical and electrical properties of F-doped ZnO nanorod semiconductor thin films deposited by sol–gel process, Appl. Surf. Sci. 255 (2008) 2353–2359.
[7] E.J. Luna-Arredondo, A. Maldonado, R. Asomoza, D.R. Acosta, M.A. Meléndez-Lira, M. dela L. Olveraa, Indium-doped ZnO thin films deposited by the sol–gel technique, Thin Solid Films 490 (2005) 132–136.
[8] Krisana Chongsri, Chatpong Bangbai, Wicharn Techitdheera, Wisanu Pecharapa, Characterization and photoresponse properties of Sn-doped ZnO thin films, Energy Procedia 34 (2013) 721–727.

[9] S. Lima, M. Davolos, C. Legnani, W. Quirino, M. Cremona, Low voltage electroluminescence of terbium- and thulium-doped zinc oxide films, J. Alloys Compd. 418 (2006) 35–38.
[10] P. Chen, X. Ma, D. Yang, ZnO: Eu thin-films: Sol–gel derivation and strong photoluminescence from $^5D_0 \rightarrow {}^7F_0$ transition of E^{3+} ions, J. Alloys Compd. 431 (2007) 317–320.
[11] Ravinder Kaur, A.V. Singh, R.M. Mehra, Sol–gel derived highly transparent and conducting yttrium doped ZnO films, J. Non-Cryst. Solids 352 (2006) 2335–2338.
[12] Jinghai Yanga, Rui Wanga, Lili Yanga, Jihui Langa, Maobin Weia, Ming Gaoa, Xiaoyan Liua, Jian Caoa, Xue Li, Nannan Yang, Tunable deep-level emission in ZnO nanoparticles via yttrium doping, J. Alloys Compd. 509 (2011) 3606–3612.
[13] Sungeun Heo, Sanjeev K. Sharma, Sejoon Lee, Youngmin Lee, Changmin Kim, Byungho Lee, Hwangho Lee, Deuk Young Kim, Effects of Y contents on surface, structural, optical, and electrical properties for Y-doped ZnO thin films, Thin Solid Films 558 (2014) 27–30.
[14] R. Mariappan, V. Ponnuswamy, A. ChandraBose, R. Suresh, M. Ragavendar, Influence of Y doping concentration on the properties of nano structured $M_X\ Zn_{1-X}\ O$ (M=Y) thin film deposited by nebulizer spray pyrolysis technique, J. Phys. Chem. Solids 75 (2014) 1033–1040.
[15] Yu-Zen Tsai, Na-Fu Wang, Mei-Rurng Tseng, Feng-Hao Hsu, Transparent conducting Al and Y codoped ZnO thin film deposited by DC sputtering, Mater. Chem. Phys. 123 (2010) 300–303.
[16] Feng-Hao Hsu, Na-Fu Wang, Yu-Zen Tsai, Mau-Phon Houng, A novel Al and Y co-doped ZnO/n-Si hetero-junction solar cells fabricated by pulsed laser deposition, Sol. Energy 86 (2012) 3146–3152.
[17] Necmettin Kılınç, Sadullah Öztürk, Lütfi Arda, Ahmet Altındal, Zafer Ziya Öztürk, Structural, electrical transport and NO_2 sensing properties of Y-doped ZnO thin films, J. Alloys Compd. 536 (2012) 138–144.
[18] S. Anandan, S. Muthukumaran, Influence of Yttrium on optical, structural and photoluminescence properties of ZnO nanopowders by sol–gel method, Opt. Mater. 35 (2013) 2241–2249.
[19] B.D. Cullity, Elements of X-ray Diffractions, Addison-Wesley, Reading, MA, 1978.
[20] Hyung WooChoi, Kyu-Sung Lee, N. David Theodore, T.L. Alford, Improved performance of ZnO nanostructured bulk heterojunction organic solar cells with nanowire-density modified by yttrium chloride introduction into solution, Sol. Energy Mater. Sol. Cells 117 (2013) 273–278.
[21] Anubha Jain, P. Sagar, R.M. Mehra, Band gap widening and narrowing in moderately and heavily doped n-ZnO films, Solid-State Electron. 50 (2006) 1420–1424.
[22] E. Burstein, Anomalous optical absorption limit in InSb, Phys. Rev. 93 (1954) 632–701.
[23] B. Lin, Z. Fu, Y. Jia, Green luminescent center in undoped zinc oxide films deposited on silicon substrates, Appl. Phys. Lett. 79 (2001) 943–945.
[24] K. Vanheusden, C.H. Seager, W.L. Warren, D.R. Tallant, J.A. Voigt, Mechanisms behind green photoluminescence in ZnO phosphor powders, J. Appl. Phys. 79 (1996) 7983–7990.
[25] K.J. Chen, F.Y. Hung, S.J. Chang, S.J. Young, Optoelectronic characteristics of UV photodetector based on ZnO nanowire thin films, J. Alloys Compd. 479 (2009) 674–677.
[26] J. Liu, C. Zhao, Z. Li, J. Chen, H. Zhou, S. Gu, Y. Zeng, Y. Li, Y. Huang, Low-temperature solid-state synthesis and optical properties of CdS–ZnS and ZnS–CdS alloy nanoparticles, J. Alloys Compd. 509 (2011) 9428–9433.
[27] Qingjiang Yu, Haibin Yang, Wuyou Fu, Lianxia Chang, Jing Xu, Cuiling Yu, Ronghui Wei, Kai Du, Hongyang Zhu, Minghui Li, Guangtian Zou, Transparent conducting yttrium-doped ZnO thin films deposited by sol–gel method, Thin Solid Films 515 (2007) 3840–3843.